Supporting Information Appendix

SI Materials and Methods

Patients. From 2007 to 2016, 61 adults T-ALL patients were diagnosed in RuiJin Hospital Affiliated to Shanghai JiaoTong University School of Medicine, the First Affiliated Hospital of Soochow University, and the Fujian medical University Union Hospital, and 69 pediatric T-ALL patients were diagnosed in Shanghai Children's Medical Center according to the WHO criteria. All the data were re-reviewed by the evaluation group of Shanghai Institute of Hematology (SIH). The study was approved by the ethical board of the participating centers. All patients were given informed consent for both treatment and cryopreservation of bone marrow (BM) and peripheral blood samples according to the Declaration of Helsinki.

Treatment. Adult patients in discovery cohort were mostly enrolled in an SIH protocol (Chinese Clinical Trial Registry, number ChiCTR-RNC-14004969 for sample collection and ChiCTR-ONRC-14004968 for treatment respectively), which was a protocol similar to CALGB 8811 induction chemotherapy (Larson regimen), based on a modification of M.D. Anderson consolidation regimen (Hyper-CVAD, alternating with high-dose methotrexate and cytarabine for 4 cycles)(1, 2). We carried on weekly methotrexate, daily 6-MP and monthly vincristine/prednisone pulses for 2 years as maintenance regimen.

Pediatric patients in discovery cohort were mostly enrolled in the Shanghai Children's Medical Center ALL-2005 protocol (Chinese Clinical Trial Registry, numberChiCTR-ONC-14005003). This protocol was a modified ALL-XH-99 regimen(3). The most important change was to move the high-dose Ara-C from the consolidation treatment to the later maintenance in the intermediate-risk and high-risk groups, whereas conventional dosage (Ara-C 100 mg/m2/day, q12h, H, d1-7) was still used in the consolidation treatment in low-risk group(4).

RNA sequencing alignment. RNA sequencing were performed in all 130 patients according to previously described method(5). RNA-seq data were aligned against the human reference genome hg19 using Hisat2 (Version 2.0.5)(6). HTSeq was used to generate a counts table from Hisat2 output(7).

Fusion detection by RNA-seq and confirmation using Reverse transcription polymerase chain reaction (RT-PCR). FusionCatcher (Version 0.99.3d)(8) and Defuse (Version 0.6.2)(9) were used for finding somatic fusion genes such that there were at least 2 split reads and 3 spanning reads in the analyzed RNA-seq data. RT-PCR was performed to examine the newly identified fusion genes which had not been previously reported and 18 novel fusions were confirmed. For the fusions that may result in fusion proteins, we further estimated their impact to the ORFs based on the predicted break points and adjacent sequences.

Whole exome sequencing alignment. Whole exome sequencing was performed in 36 patients without fusion genes, 16 individuals having their own normal control samples (blood samples in CR). Read pairs were aligned to the human reference genome (hg19, downloaded from the UCSC Genome Browser) by BWA (version 0.7.15-r1140). Samtools (version 1.3) were applied to generate chromosomal coordinate-sorted bam files. Alignment files were processed further with the Picard (version 1.138) and GATK before variant calling. Duplicate removal, local realignment around known indels and base quality recalibration were performed. These data were compared to RNA-seq data from the same samples from 36 cases. Among genes with mutation rates >3%, 123/125 (98.4%) of the sequencing variations detected in RNA-seq were also found in WES, confirming the validity of our RNA-seq based mutation calling system.

Mutation calling from RNA-seq data. A recent publication using RNA-seq to identify mutations in a large B-ALL series was taken as reference(10, 11). As in their reports, several gene mutations (like *NOTCH1*, *FBXW7*, *PTEN*, *NRAS, KRAS, JAK2, IKZF1*, *CREBBP*, *RPL10* etc.) were found using RNA-seq and confirmed by partial WES or Sanger sequencing. Based on RNA-seq and WES data from our previous work or public database, more stringent procedure to rule out rare SNPs were applied in this study. The mutations were called according to the GATK forum recommended pipeline for calling variant in RNA-seq data(12). Specifically, STAR (version 2.5.2b) mapped bam files were processed by Picard(13). Variant calling was performed by the HaplotypeCaller, UnifiedGenotyper module in GATK, VarScan2 and LoFreq(14, 15), then the variants were quality controlled by the following steps: (1) at least three reads supported the mutation and the mutant allele frequency was >5% or be validated by Sanger sequencing; (2) not observed in common dbSNP 147 database or presented in the 1000 Genomes Project database; (3) sequence variation frequency <=2 in normal control samples [blood in complete remission (CR), saliva, and skin tissues] from 265 ALL and lymphoma cases in our previous publications(5, 16) and this work; (4) supported by double strand of the genome; (5) not found in DARNED and RADAR RNA-editing database(17, 18). After filtering, all the mutations were annotated to genes according to their genomic positions. Non-silent mutations were compared to v70 COSMIC somatic mutation database (GRCh37) for the overlapped cancer relevant genes, and to the literature for genes mutated in T-ALL(19-22).

In 36 cases with WES data, 95.5% of recurrent gene abnormalities including loss-of-function mutations in TSGs of WES data were also found by RNA-seq analysis, suggesting no obvious decay of genetic information in the latter setting in T-ALL.

Gene expression and pathway analysis. The mRNA expression levels in transcriptome sequencing data were estimated as FPKM values. Briefly, read counts in the corresponding GENCODE annotated gene model were obtained with the HTseq-count program. FPKM values were computed by normalizing the obtained read counts for a transcript or gene with the length of the transcript or gene and the total mapped reads. All gene expression data from RNA-seq experiments were normalized together using variance stabilizing transformation in the DESeq2 package to remove any technical or spurious background variation(23). The top 1,484 genes (about 10 percent) were selected only based on the highest variability of gene expression across samples. Unsupervised hierarchical clustering was performed with ward method in R “gplots” package. The distance was based on the Pearson correlation coefficient.

RNA splicing and aberrant transcript analysis. Read counting was performed using HTSeq-count 0.9.1 (http://htseq.readthedocs.io/en/release_0.9.1/) with custom Python scripts provided by the DEXSeq(24). Read count tables and group comparisons for differential exon or transcript usage were performed with DEXSeq. Exon bins after the quantification has been filtered to improve reliability of differential exon usage. The filter method was according to previous published paper (25).

Multiplex ligation-dependent probe amplification (MLPA). Multiplex ligation-dependent probe amplification is an attractive property for copy number variation analysis (26). Hybridization and ligation steps were performed on 100 ng genomic DNA, and probes were subjected to PCR reactions using SALSA ME024 9q21 *CDKN2A/2B* region probemix according to the manufacturer's instructions (MRC-Holland). Targeted loci included 9p21 region encompassing the *CDKN2A/2B* gene. Products were run on ABI 3730XL genetic analyzer.

SNP array analysis. Total genomic DNA (200ng) was amplified, randomly fragmented and hybridized to Affymetrix Axiom 2.0 Assay according to the manufacturer's protocol. The hybridization, washing and scanning were completed in the Affymetrix GeneTitan MC instrument. The raw data (*.CEL) files were analyzed using the Axiom™ Analysis Suite (Version 2.0.0.35) of Affymetrix. Log R Ratio (LRR) and B Allele Frequency (BAF) were calculated by Axiom CNV Tool (Version 1.1.0.85). Affymetrix official annotation file (Axiom_PMRA.na35.annot.db) was combined as the input data. The output file (*.PennCNV) were analyzed by PennCNV (Version 1.0.3) and GFD(27).

Plasmid construction. The wild-type *ZBTB16* and *ABL1* cDNA clones were kindly provided by OriGene. The *ZBTB16-ABL1* fusion cDNA was constructed into the XhoI and EcoRI multiple cloning sites of retroviral vector MSCV-IRES-GFP (Migr1). All recombinant plasmids were verified by DNA sequencing.

Cell transfection. Purified plasmids Migr1-vector or Migr1-*ZBTB16-ABL1* were cotransfected into HEK-293T cells with packaging vectors with Lipofectamine 2000 (Invitrogen) according to the manufacturer's protocol. The HEK-293T cell culture supernatants were then concentrated to a viral concentration of approximately 3×10^8 TU/ml. The viral particles were incubated with Jurkat cells for 4 h. The stably transfected clones were selected by GFP.

Cell proliferation assay. The stably transfected Jurkat cells were seeded in 96-well plates at a certain density per well. After incubation for 48 hours, cell proliferation was monitored by using the CellTiter-Glo® Luminescent Cell Viability Assay (Promega Corporation) following the manufacturer's instruction.

Cell cycle analysis. The stably transfected Jurkat cells were fixed in cold 70% ethanol, washed once in PBS, and re-suspended in PBS supplemented with 100 μg/ml DNase-free RNase A (QIAGEN) and 100 μg/ml propidium iodide (PI)

(Sigma). Samples were processed using the LSR Fortessa^{TM} X-20 flow cytometer (BD Biosciences) according to the manufacturers' instructions.

Protein tyrosine kinase assay. ABL1, ZBTB16-ABL1 (ZA) and BCR-ABL (BA) tyrosine kinase activity were measured using universal tyrosine kinase assay kit (Takara) according to the manufacturer's instructions. Briefly, the HEK-293T cells were transfected with Migr1-vector, Migr1-ZBTB16-ABL1 or Migr1-BCR-ABL (provided by Jian-Hua Mao, Shanghai Institute of Hematology) plasmids. Cell lysates were prepared and the ABL1 antibody (Cell Signaling, 2862; 1:100 dilution) was used for immunoprecipitation. Agarose beads conjugated with protein A/G were added. The amounts of ABL1 proteins of ABL1, ZA and BA were normalized and the immunoprecipitates were then incubated with ATP-2Na in immobilized wells. Horseradish peroxidase-conjugated antiphosphotyrosine (PY20) antibody was added to each well and developed by addition of HRP substrate solution (TMBZ). The reaction was stopped with 1N H_2SO_4 and absorbance was measured at 450 nm on a spectrophotometer. Each test was triplicated and the results were calibrated with a corresponding phosphopeptide standard curve and control.

Cellular drug inhibition assay. Imatinib and dasatinib were purchased from Selleck. Both drugs were stored at -20^{o}C as a 10mM stock solution in dimethyl sulfoxide (DMSO). The stably transfected Jurkat cells were plated at 1×10^4 cells per well in 96-well plates in PRMI-1640 medium supplemented with 10% heat-inactivated FBS. TKIs were included in media at increasing concentrations. Viable cell number was assessed 48h postplating using the CellTiter-Glo Luminescent Cell Viability Assay (Promega) according to the manufacturer's instructions. All experiments were performed intriplicate.

Mouse keeping, retrovirus packaging, BM transplantation. Mice used in this study were housed in the specific pathogen free circumstance in Research

Center for Experimental Medicine in RuiJin Hospital Affiliated to Shanghai Jiao Tong University School of Medicine. Male BALB/c mice (aged 6–8 weeks, *n*=10) and female BALB/c mice (aged 6–8 weeks, *n*=20) were raised in a temperature (22±1°C) and humidity (55±5%) controlled room with 12 hours of light and 12 hours of dark a day. All animal experiments were conducted following the institutional ethical guidelines on animal care and were approved by the Animal Care and Use Committee of Shanghai Jiao Tong University School of Medicine. Retroviral supernatants were generated by co-transfecting 293T cells with recombinant plasmids and ecopac retroviral packaging plasmid using Lipofectamine 2000 (Invitrogen). BM cells were isolated from male BALB/c mice that received 5-fluorouracil (250 mg/kg) 5 days before harvest. The primary murine BM cells were then infected once a day for 2 days with a retroviruses mixture consisting of DMEM supplemented with 15% FBS, IL-3 (10 ng/mL), IL-6 (10 ng/mL), IL-7 (10 ng/mL), Flt3L (10 ng/mL), SCF (50 ng/mL) and polybrene (5ug/mL). All cytokines were obtained from R&D Systems. After 24-hour infection, cells were randomly injected into lethally irradiated recipient female BALB/c mice through the tail vein (*n*=10 for each group). Two weeks after transplantation, peripheral blood was collected to analyze the percentage of GFP positive cells to evaluate the efficiency of transplantation.

***In vivo* treatment studies.** The primary bone marrow transplantation mouse model was used. Dasatinib or imatinib treatment was started 10 days after transplantation. Imatinib was dissolved at 10 mM in 100% dimethyl sulfoxide (DMSO) and formulated in 5% carboxymethylcellulose solution and given in a dose of 50 mg/kg. Dasatinib was dissolved in H_2O and given in a dose of 5 mg/kg. Control mice were treated with equal volumes of vehicle (carboxymethylcellulose and H_2O). Drugs or vehicle was given by oral gavage twice per day for 5 days followed by a 2-day rest in a volume of 0.01 mL/g of mouse body weight. The treatment continued until the death of the control mice.

Morphological and immunophenotypic analysis. Peripheral blood cell counts were performed with a Poch-100iv Diff (Sysmex Corp). Smears and cytospin preparations were subject to Wright's staining for routine cell morphology. For immunophenotyping, after lysis of red blood cells, white blood cells were incubated for 30 minutes with antibodies against Gr-1, Mac-1, CD3, B220, CD117 or cocktail of lineage antibodies purchased from BD Pharmingen or eBioscience. The cells then were spun down, re-suspended in 200 μL PBS, and analyzed on LSR Fortessa^{TM} X-20 (BD Biosciences).

Statistical analysis. The differences in cell proliferation between different groups were statistically analyzed by using an unpaired Student's *t* test. Comparisons of categorical variables were determined by Pearson's Chi-square test or Fisher's exact test. The OS and EFS were estimated by Kaplan-Meier method and compared by log-rank test. OS was defined as from the diagnosis of the disease to death or alive at last follow-up (censored); EFS was from disease diagnosis to treatment failure such as relapse, death, or alive in CR at last follow-up (censored). The last follow-up was carried out on February 2017. *P* values <0.05 were considered statistically significant. All statistical procedures were performed with the GraphPad Prism 5, R3.2.2 or SPSS Version 22.0 statistical software.

SI Figures

Figure S1. Kaplan-Meier survival curves of adult (>=18 years) and pediatric (<18 years) T-ALL patients.

(**a**) OS of children and adults with T-ALL, *P*<0.0001. The 3-year-OS of pediatric patients was 72.8% (95% CI 67.3-78.3), and the 3-year-OS rate of adult patients was 29.0% (95% CI 22.4-35.6). (**b**) RFS of children and adults with T-ALL, *P*<0.0001. The 3-year-EFS of pediatric patients was 70.7% (95% CI 65.2-76.2), and the 3-year-EFS of adult patients was 18.6% (95% CI 12.9-24.3).

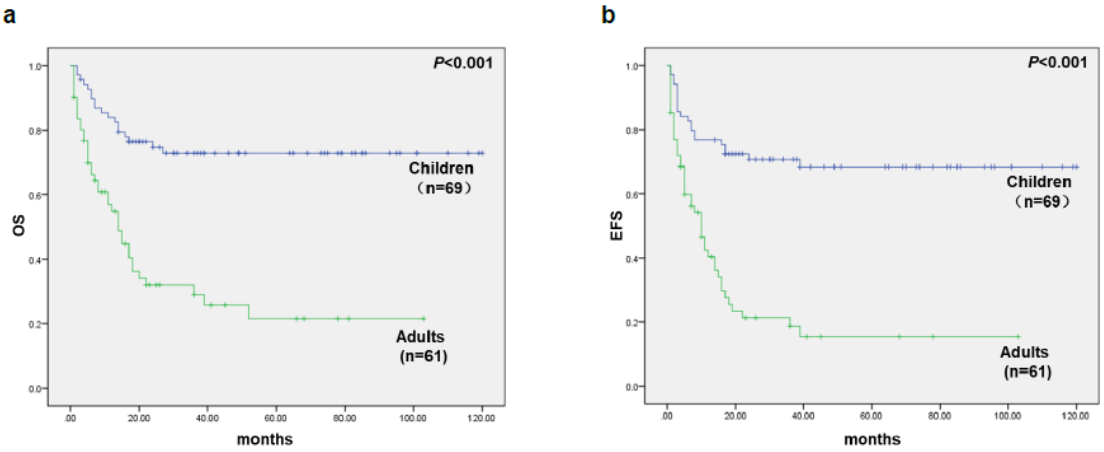

Figure S2. Novel identified 18 rearrangements in 130 T-ALL patients. Predicted domain structure of four type fusion genes. Type1 included *SLC38A2-ABL2*, *GNPTAB-ATF7IP*, *ARL8A-INSRR*, *MELK-SIK3*, *MBNL1-TAL1*, *ZBTB16-ABL1*, *MYH9-JAK2*, *EEFSEC-PDHX*, *MBNL1-ANXA3*, *NUP98-VRK1*, and *IKZF1-NOTCH1*. Type2 included *CCND3-STIL*, *EVL-NKX2-1* and *EVL-SFTA3.* Type3 included *ZFP36L2-TRA*, *TRB-AHI1*, *TRA-SALL2* and *TRD-NKX2-1.* Type4 included *PPP4R3A-IGH*. The main domains of the protein structure information were extracted from the UniProt and NCBI conserved domain databases. *EVL-NKX2-1* and *EVL-SFTA3* were located in the same case C47. *EVL-SFTA3* probably caused by a splicing between *EVL* and *SFTA3*, which is located just downstream to *NKX2-1*. We counted *EVL-NKX2-1* and *EVL-SFTA3* as one novel fusion event.

Type 1

Case ID: A5 Fusion: *SLC38A2-ABL2* Frame info: in-frame

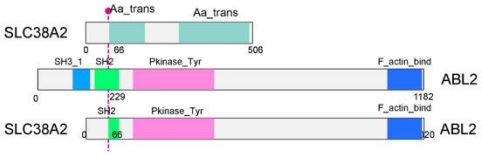

Case ID: A22 Fusion: *GNPTAB-ATF7IP* Frame info: in-frame

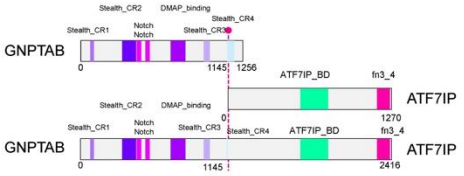

Case ID: A38 Fusion: *ARL8A-INSRR* Frame info: in-frame

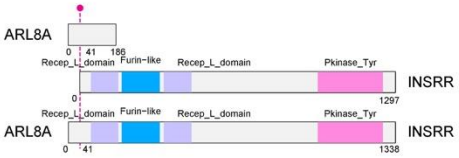

Case ID: C1 Fusion: *MELK-SIK3* Frame info: in-frame

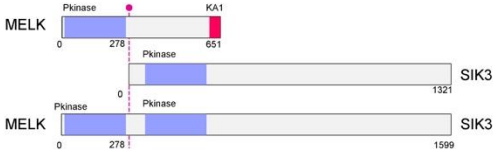

Case ID: C6 Fusion: *MBNL1-TAL1* Frame info: in-frame

Case ID: C11 Fusion: *ZBTB16-ABL1* Frame info: in-frame

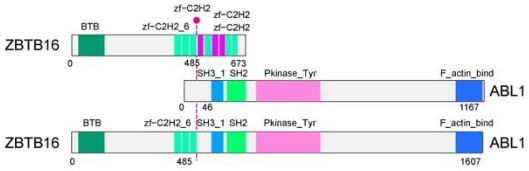

Case ID: C23 Fusion: *ZBTB16-ABL1* Frame info: in-frame

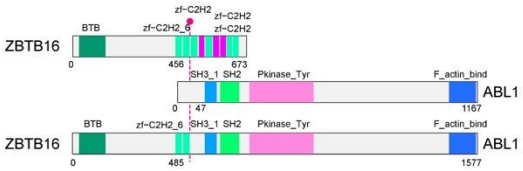

Case ID: C20 Fusion: *MYH9-JAK2* Frame info: in-frame

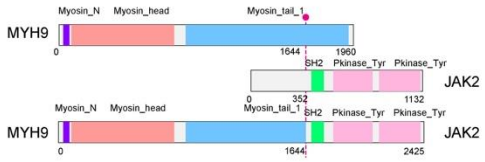

Case ID: C25 Fusion: *EEFSEC-PDHX* Frame info: in-frame

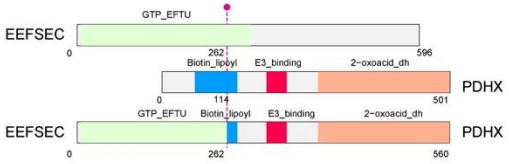

Case ID: C31 Fusion: *MBNL1-ANXA3* Frame info: in-frame

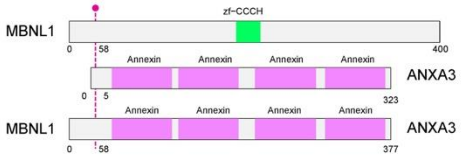

Case ID: C43 Fusion: *NUP98-VRK1* Frame info: in-frame

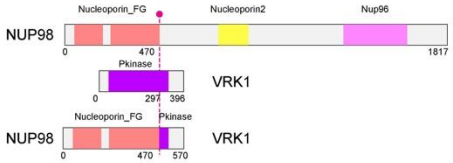

Case ID: C63 Fusion: *IKZF1-NOTCH1* Frame info: in-frame

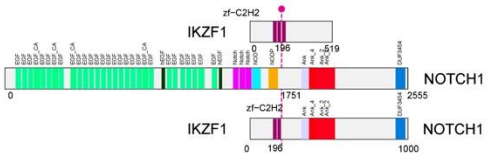

Type 2

Case ID: A36 Fusion: *CCND3-STIL* Frame info: in-frame

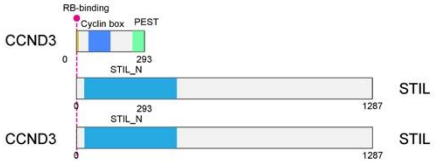

Case ID: C47 Fusion: *EVL-NKX2-1* Frame info: in-frame

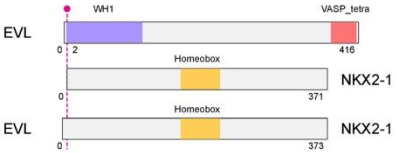

Case ID: C47 Fusion: *EVL-SFTA3* Frame info: in-frame

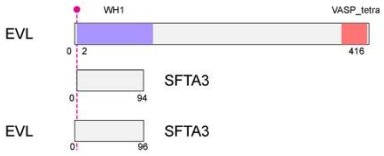

Type 3

Case ID: A25 Fusion: *ZFP36L2-TRA* Frame info: UTR/---

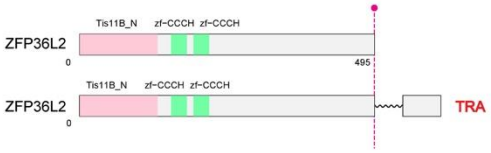

Case ID: C17 Fusion: *TRB-AHI1* Frame info: ---/CDS

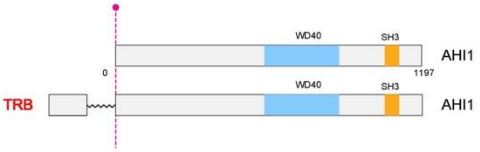

Case ID: C22 Fusion: *TRA-SALL2* Frame info: ---/CDS

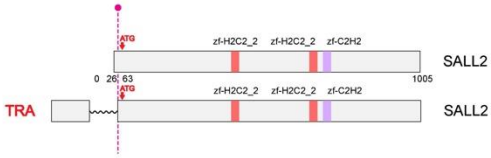

Case ID: C38 Fusion: *TRA-SALL2* Frame info: ---/CDS

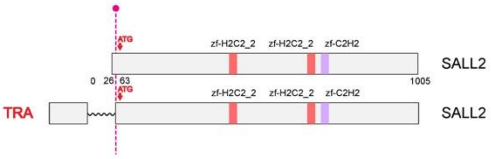

Case ID: C55 Fusion: *TRD-NKX2-1* Frame info: ---/UTR

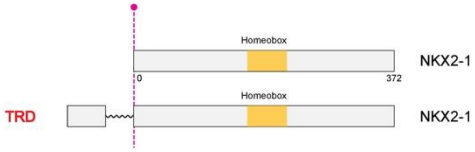

Type 4

Case ID: C60 Fusion: *PPP4R3A-IGH* Frame info: intronic/---

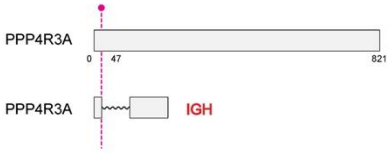

Figure S3. *EVL*, *NKX2−1* and *SALL2* gene expression levels in 130 T-ALL patients.

T-ALL cases in G1, G2 and G3 groups were shown in different colors. (**a**) *EVL* was highly expressed in 130 T-ALL patients. (**b**) *NKX2-1* was highly expressed in cases with *TRD-NKX2-1* and *EVL-NKX2-1* fusions. (**c**) Cases with *TRA-SALL2* fusions had higher expression of *SALL2* than others.

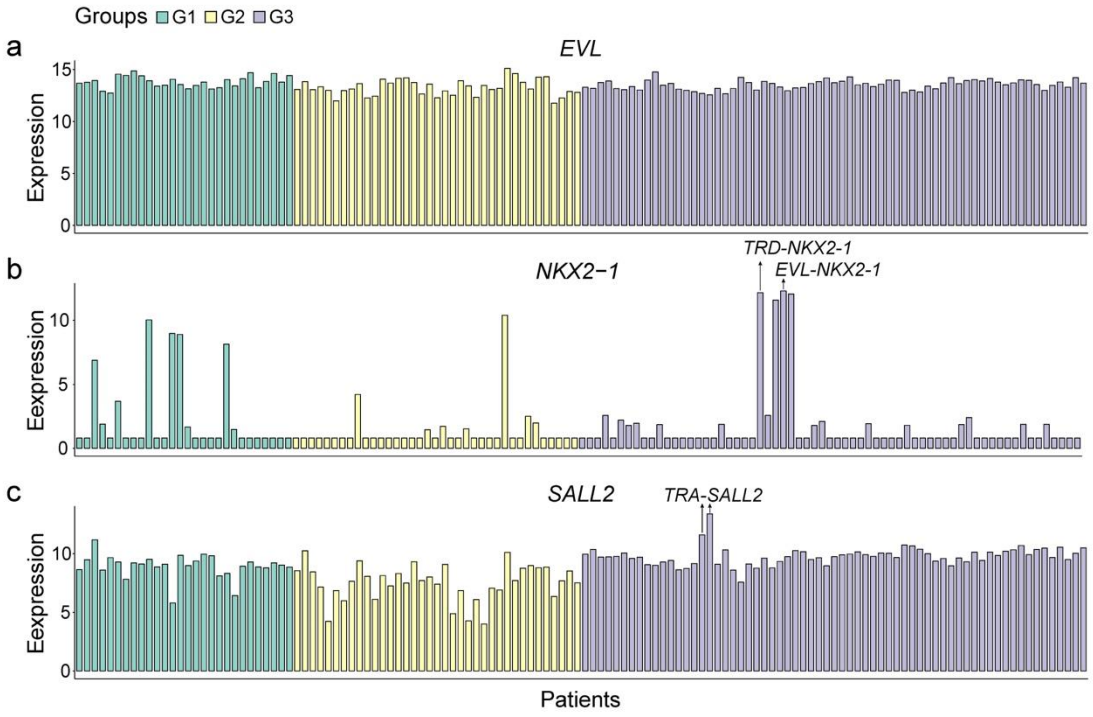

Figure S4. Phenotypic and morphological analysis of *ZBTB16-ABL1* (ZA) mice.

(**a**) Average percent of GFP^+ cells in PB after BMT. (**b**) Histogram of WBC counts in control and ZA mice. (**c**) Histogram of the relative proportions of cells with different populations of BM cells of ZBTB16-ABL1 (ZA) mice and control mice as determined by morphological analysis. (**d**) Spleen weight/body weight of control and ZA mice. Scale bar, 1 cm. (**e**) Liver weight/body weight of control and ZA mice. Scale bar, 1 cm. (**f**) Wright staining of BM cytospin samples from ZBTB16-ABL1 (ZA) mice and control. Scale bar, 15 μm. (**g**) Morphological comparison of PB in control and ZA mice. Scale bar, 10 μm. (**h**) Wright staining of cytospin of spleen from control and ZA mice. Scale bar, 10 μm. (**i**) Representative flow cytometric analysis of GFP-expressing BM cells for Gr-1 and Mac-1 in ZBTB16-ABL1 (ZA) versus control. Error bars represent mean ± s.d. (n=4-10 recipients per group). ***P<0.001. Statistical significance was determined using two-sided Student's t test.

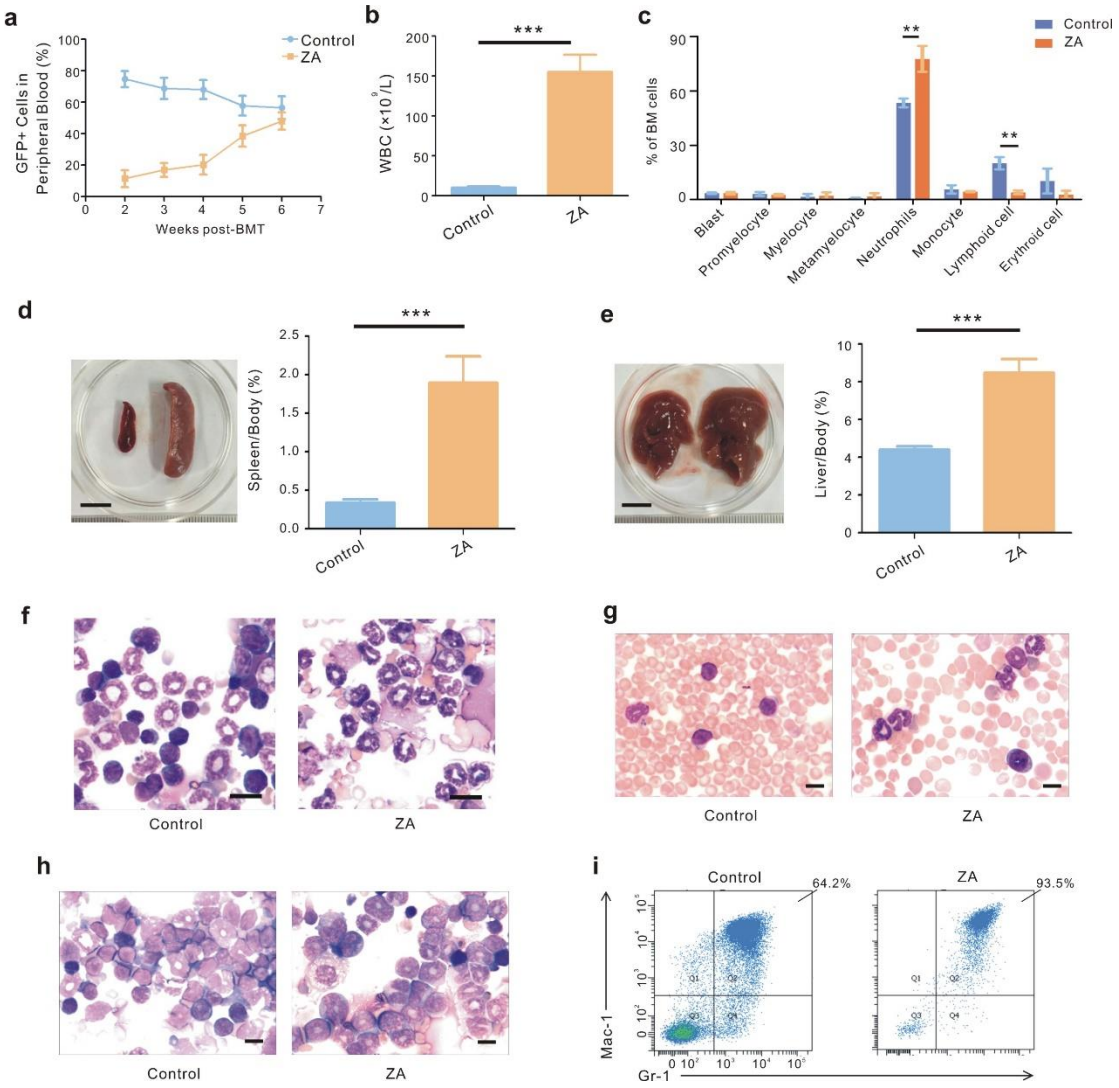
a
GFP+ Cells in Peripheral Blood (%)
Control
ZA
Weeks post-BMT
b
WBC (×10⁹/L)
***
Control
ZA
c
% of BM cells
Control
ZA
**
**
Blast
Promyelocyte
Myelocyte
Metamyelocyte
Neutrophils
Monocyte
Lymphoid cell
Erythroid cell
d
Spleen/Body (%)
***
Control
ZA
e
Liver/Body (%)
***
Control
ZA
f
Control
ZA
g
Control
ZA
h
Control
ZA
i
Control
64.2%
ZA
93.5%
Mac-1
Gr-1

Figure S5. Unsupervised hierarchical clustering of global gene expression profile from 130 T-ALL patients. Columns indicate individual T-ALL patients, and rows represent 1,484 most variably expressed genes on autosomal chromosome according to RNA-seq data. Gene over-expression and under-expression status are shown in red and green, respectively. Three major T-ALL groups are identified on the basis of gene expression profiles. Group 3 can be further divided into G3a and G3b subgroups.

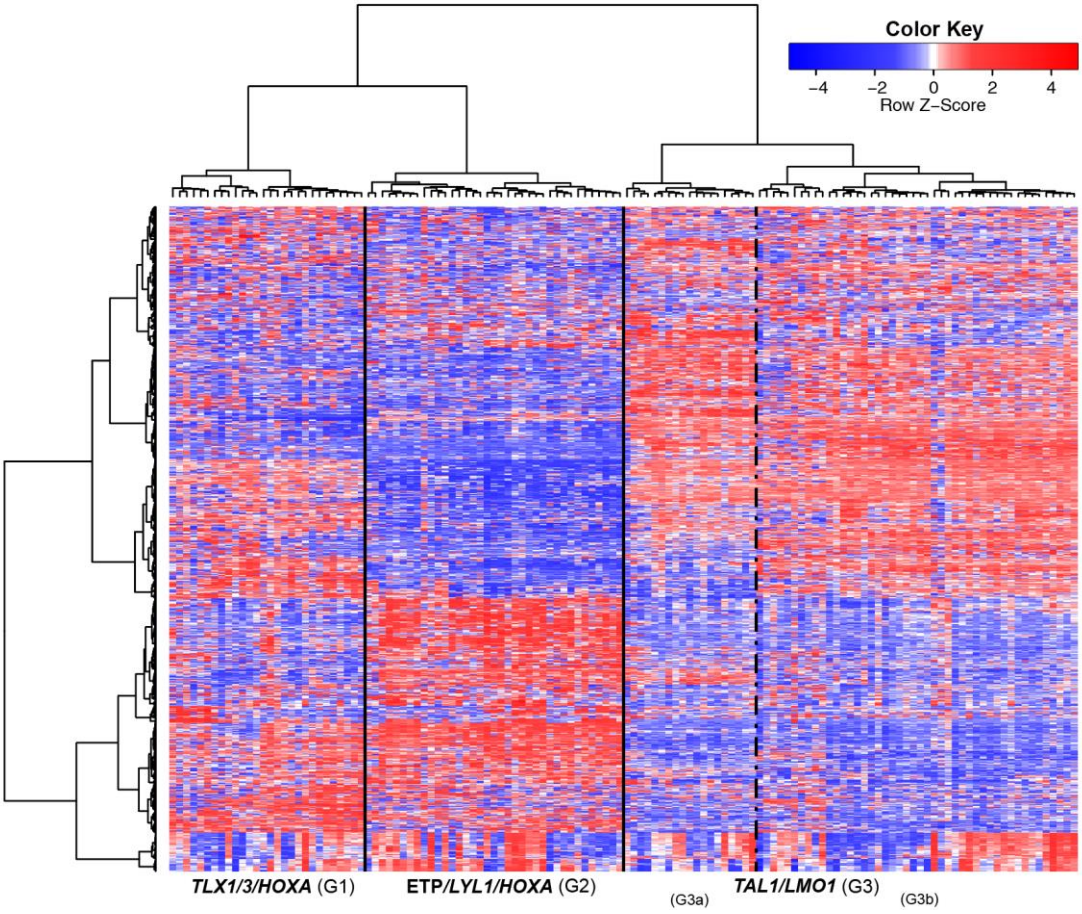

Figure S6. Gene functional analysis of expression profile for each group. Gene ontology (GO) analysis of the up-regulated genes in each transcriptome-based group (G1, G2 and G3) was performed with Database for Annotation Visualization and Integrated Discovery (DAVID) v6.8. KEGG pathways enrichment $\log_{10}$ transferred P-Values were shown as bar plot. G1, G2 and G3 functional enrichment results were listed below as (**a**), (**b**) and (**c**), respectively.

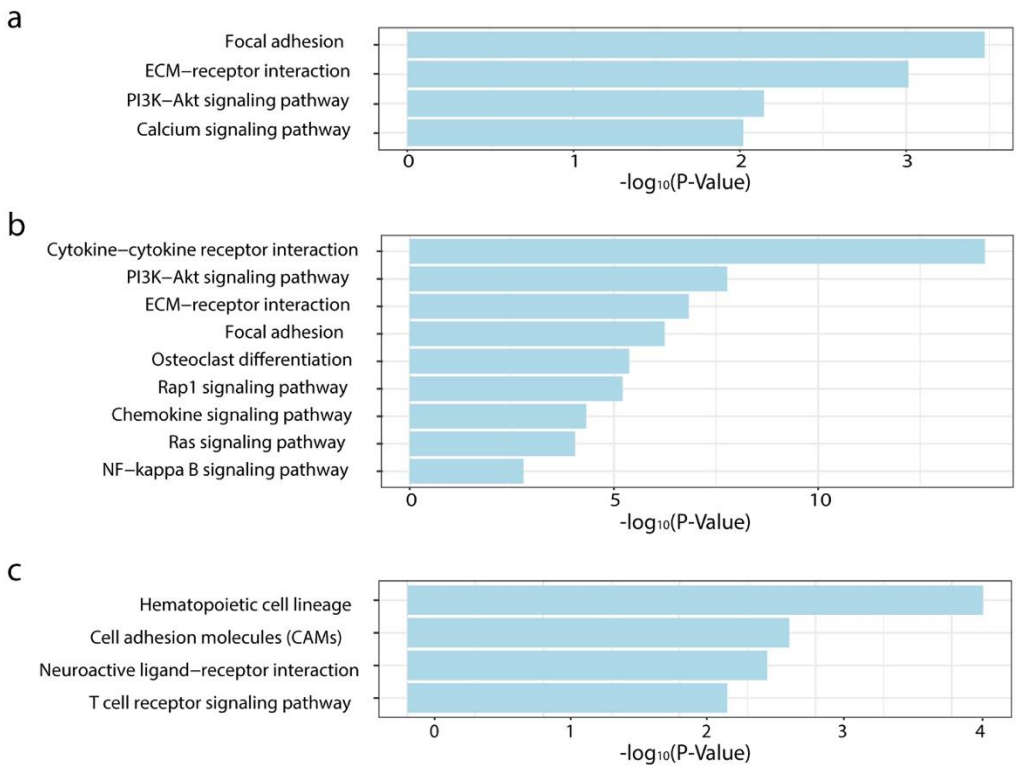

Figure S7. Aberrant *SLC17A9* short transcript in T-ALL patients. (**a**) Coverage tracks in RNA-seq data for a *SLC17A9* wild-type case (top) and a short isoform case with deletion of exon 1-8 (bottom). (**b**) Detail of *SLC17A9* exon 9 coverage peak in the short isoform case. Amino acid information is annotated under the coverage track. (**c**) Predicted domain structure of SLC17A9 protein. Location of a putative initiation codon (methionine) in exon 9 is pointed by a green pointer.

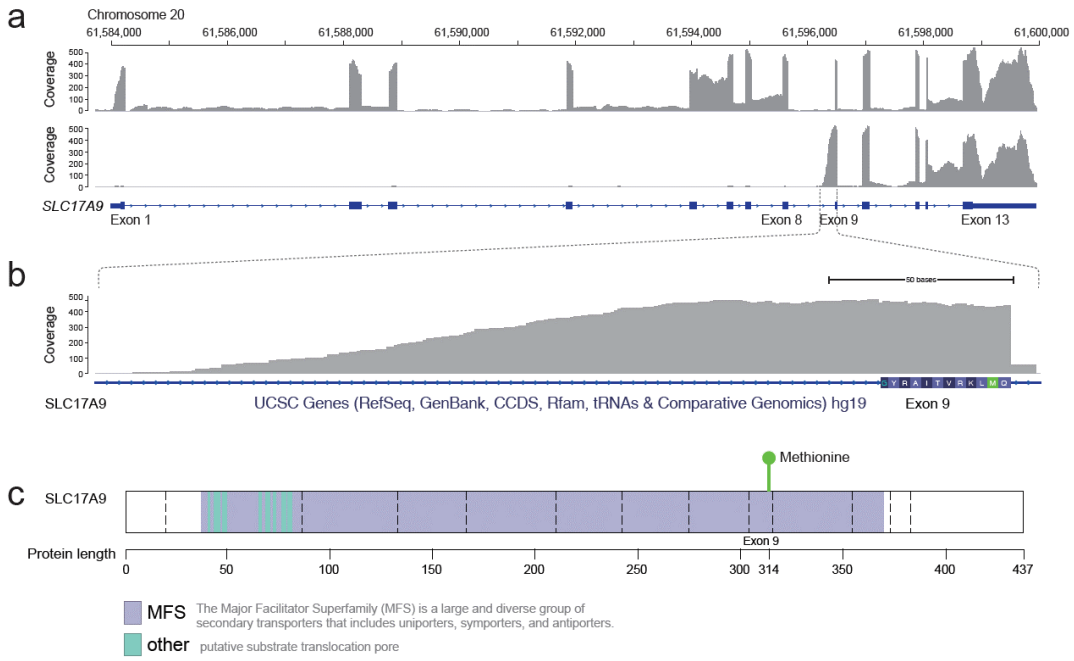

Figure S8. Schematic location of the novel gene mutations with RNA-seq and WES.

(**a**) CELSR3, (**b**) PAK4, (**c**) MINK1, (**d**) NR4A1, (**e**) BOD1L1, (**f**) VCP gene mutation sites were positioned in terms of protein structure with the main domain information according to NCBI conserved domain database. PolyPhen and SIFT were applied to the prediction of amino acid substitution to deteriorate proteins' function. For the totally 25 mutations, the prediction results of PolyPhen showed that 13 of them were "Probably damaging", 6 of them were "Possibly damaging", 4 of them were "Benign"; SIFT predicted that 12 mutations were "Damaging", 10 mutations were "Tolerated" and 3 mutations were unavailable. Especially, for the big gene *CELSR3*, all amino acid substitutions on this gene deteriorate protein' s function. The prediction results for *CELSR3* were "Possibly damaging", "Damaging", or "Tolerated" in both of PolyPhen and SIFT.

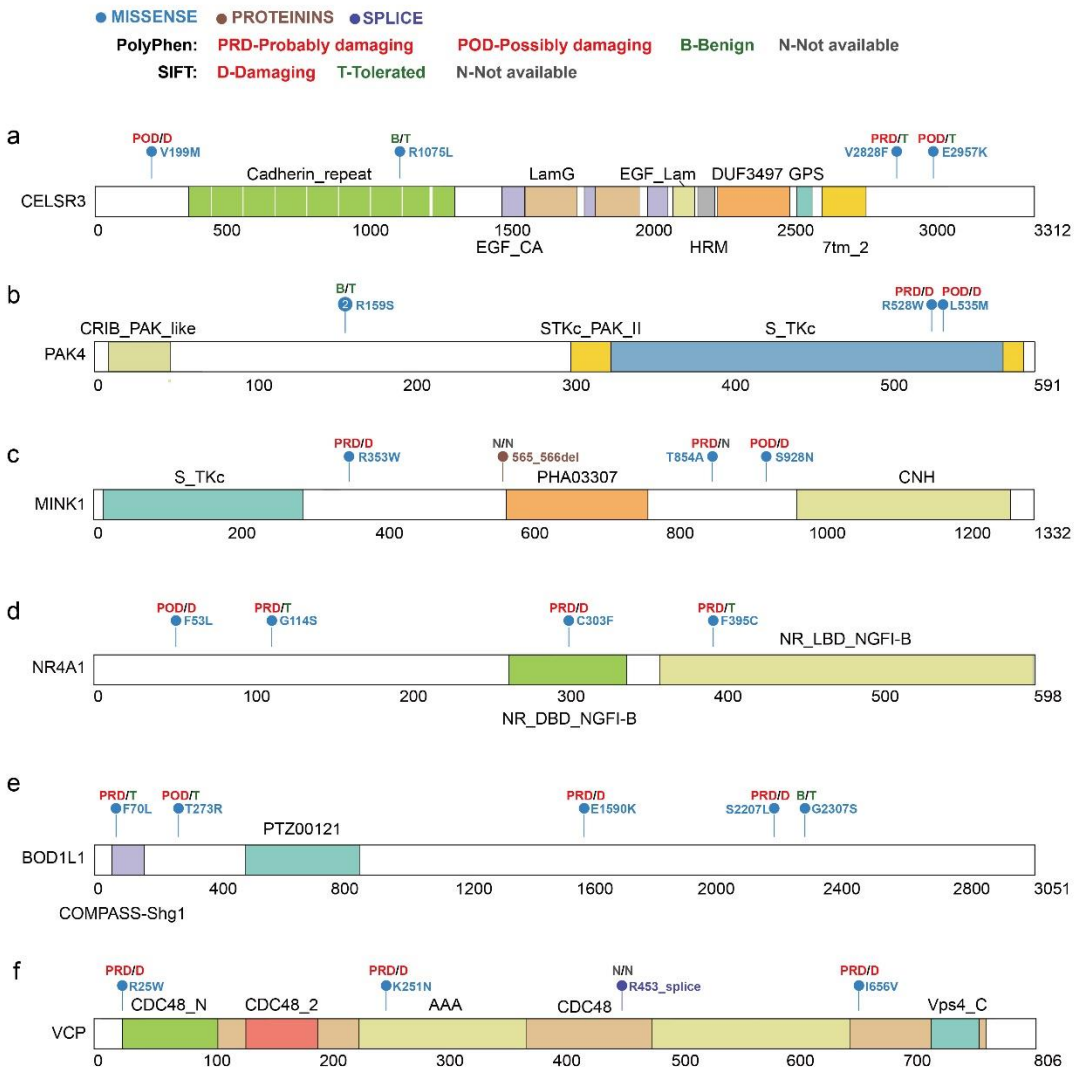
MISSENSE PROTEININS SPLICE
PolyPhen: PRD-Probably damaging POD-Possibly damaging B-Benign N-Not available
SIFT: D-Damaging T-Tolerated N-Not available
a
POD/D V199M
B/T R1075L
PRD/T V2828F
POD/T E2957K
Cadherin_repeat
LamG
EGF_Lam
DUF3497
GPS
CELSR3
0 500 1000 1500 2000 2500 3000 3312
EGF_CA
HRM
7tm_2
b
B/T R159S
PRD/D R528W
POD/D L535M
CRIB_PAK_like
STKc_PAK_II
S_TKc
PAK4
0 100 200 300 400 500 591
c
PRD/D R353W
N/N 565_566del
PRD/N T854A
POD/D S928N
S_TKc
PHA03307
CNH
MINK1
0 200 400 600 800 1000 1200 1332
d
POD/D F53L
PRD/T G114S
PRD/D C303F
PRD/T F395C
NR_LBD_NGFI-B
NR4A1
0 100 200 300 400 500 598
NR_DBD_NGFI-B
e
PRD/T F70L
POD/T T273R
PRD/D E1590K
PRD/D S2207L
B/T G2307S
PTZ00121
BOD1L1
0 400 800 1200 1600 2000 2400 2800 3051
COMPASS-Shg1
f
PRD/D R25W
PRD/D K251N
N/N R453_splice
PRD/D I656V
CDC48_N
CDC48_2
AAA
CDC48
Vps4_C
VCP
0 100 200 300 400 500 600 700 806

Figure S9. The correlation between mutation counts and age.

(a) Violin plot of mutation counts in adult and children (*P*=0.001). Gene mutation rates over 3% were taken into account in the comparison. **(b)** Correlation between mutation counts and age of 130 T-ALL patients subject to RNA-seq and WES that all founded mutations were included.

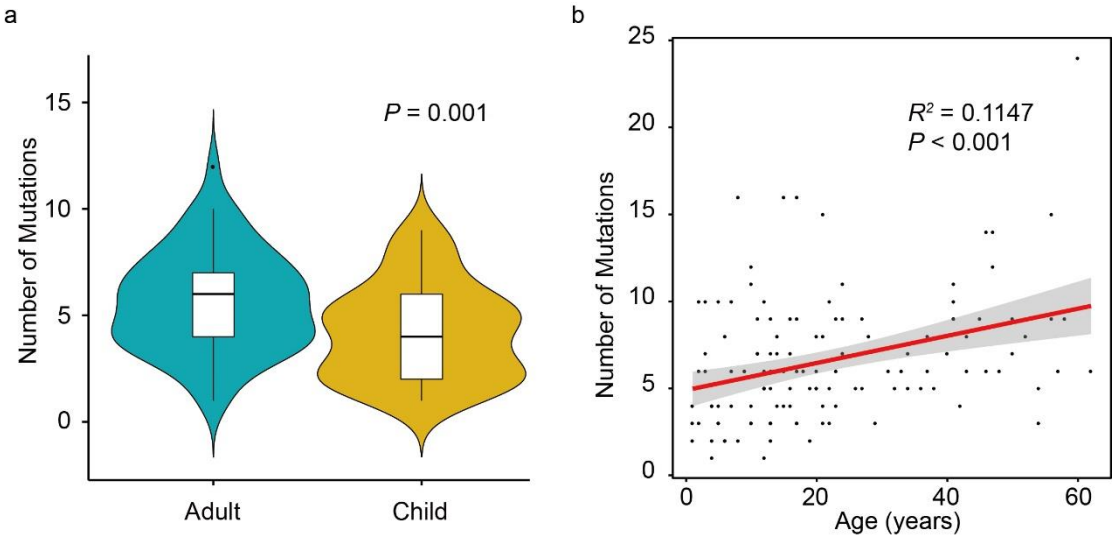

Figure S10. *MEF2C* gene expression levels in 130 T-ALL patients

T-ALL cases in G1, G2 and G3 groups were shown in different colors. The cut-off value of *MEF2C* over-expression was defined as greater than one standard deviation above mean expression (FPKM: 10.5). The corresponding horizontal red line indicated the threshold.

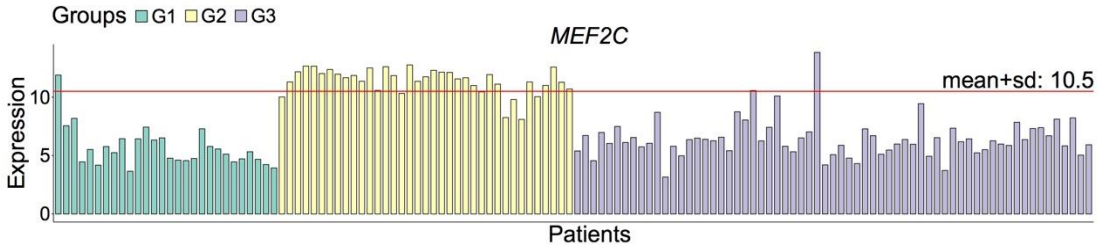

Figure S11. Kaplan-Meier survival curves of pediatric (<18 years) T-ALL patients with COG risk classification.

(**a**) OS of children with COG risk classification, *P*<0.0001. The 3-year-OS of patients with standard-, intermediate- and high-risk was 87.4% (95% CI 81.4-93.4), 64.3% (95% CI 49.7-78.9) and 12.5% (95% CI 0.8-24.2), respectively. (**b**) RFS of with COG risk classification, *P*<0.0001. The 3-year-EFS of patients with standard-, intermediate- and high-risk was 83.3% (95% CI 76.2-90.4), 51.3% (95% CI 36.7-65.9) and 12.5% (95% CI 0.8-24.2), respectively.

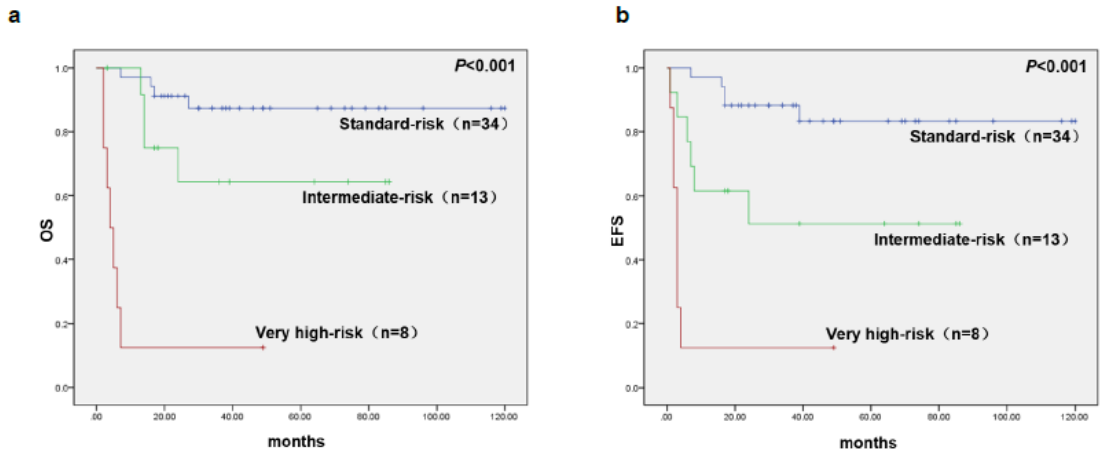

SI Tables

Table S1. Genetic characteristics of 130 patients with T-ALL

Characteristics	Group 1 (n=28)	Group 2 (n=37)	Group 3 (n=65)	*P* value
Immunophenotype [a]				
ETP	2	22	0	<0.001
Pro	1	5	3	0.172
Pre	3	8	23	0.035
Cortical	15	1	30	<0.001
Medullary	7	1	9	0.030
Fusion genes				
STIL-TAL1	0	0	20 (30.8%)	<0.001
TCR-related	0	1 (2.7%)	9 (13.8%)	0.029
LMO1/2-TRA	0	0	4	0.127
other TCR-related	0	1	5	0.217
NUP-related	3 (10.7%)	15 (40.5%)	1 (1.5%)	<0.001
SET-NUP214	0	10 (27%)	0	<0.001
NUP214-ABL1	3	1	1	0.098
NUP98-related	0	4 (10.8%)	0	0.006
KMT2A-related [b]	2	0	2	0.256
PICALM-MLLT10	3 (10.7%)	1 (2.7%)	0	0.023
ZBTB16-ABL1	0	0	2	0.362
Other fusion genes	5	3	9	0.496
Gene over-expression				
TAL1	2 (7.1%)	4 (10.8%)	24 (36.9%)	0.001
LMO1	0	2 (5.4%)	10 (15.4%)	0.040
LMO2	0	6 (16.2%)	8 (12.3%)	0.096
LYL1	4 (14.3%)	21 (56.8%)	4 (6.2%)	<0.001
HOX-related	28 (100%)	29 (78.4%)	4 (6.2%)	<0.001
TLX1	3 (10.7%)	0	0	0.004
TLX3	18 (64.3%)	0	0	<0.001
HOXA	17 (60.7%)	29 (78.4%)	4 (4.2%)	<0.001
MEF2C	1 (3.6%)	30 (81.1%)	2 (35.4%)	<0.001
Gene mutations				
NOTCH1 / *FBXW7* (C1)	26 (92.9%)	29 (78.4%)	47 (72.3%)	0.087
Signaling Pathways (C2)	17 (60.7%)	31 (83.8%)	29 (44.6%)	<0.001
JAK-STAT pathway	11 (39.3%)	19 (51.4%)	3 (4.6%)	<0.001
RAS pathway	4 (14.3%)	17 (45.9%)	4 (6.2%)	<0.001
PI3K pathway	2 (7.1%)	0	14 (21.5%)	0.004
PTEN	0	1 (2.7%)	12 (18.5%)	0.005
Epigenetic Factors (C3)	24 (85.7%)	33 (89.2%)	21 (32.3%)	<0.001
PHF6	17 (60.7%)	13 (35.1%)	1 (1.5%)	<0.001
Transcription Factors (C4)	7	14	17	0.394

[a] The immunophenotypes are classified according to the recommendation of European Group for the Immunological Characterization of Leukemias (EGIL)(28) and the National Comprehensive Cancer Network (NCCN) guideline(29). [b] *KMT2A*-related fusions include *KMT2A-MLLT1* (1 case), *KMT2A-MLLT4* (1), *KMT2A-ELL* (1), and *KMT2A-CBL* (1), respectively.

Table S2. Clinical and genetic characteristics of 130 patients with T-ALL according to Immunophenotype

Characteristics	ETP	Pro	Pre	Cortical	Medullary	*P* value
Gender, male/female	14 / 10	5 / 4	26 / 8	37 / 9	13 / 4	0.229
Age, years, Median (range)	39 (7-62)	23 (1-50)	13.5 (2-60)	15 (1-50)	16 (4-37)	
WBC count						0.007
>=100×10^9/L	2 (8.3%)	2 (22.2%)	18 (52.9%)	19 (41.3%)	8 (47.1%)	
<100×10^9/L	22 (91.7%)	7 (77.8%)	16 (47.1%)	27 (58.7%)	9 (52.9%)	
Complete Remission	17 (70.8%)	7 (77.8%)	27 (79.4%)	42 (91.3%)	17 (100%)	0.056
Relapse [a]	2 (11.8%)	2 (28.6%)	7 (25.9%)	9 (21.4%)	8 (47.1%)	0.181
Fusion genes						
STIL-TAL1	0	0	10 (29.4%)	8 (17.4%)	2 (11.8%)	0.022
TCR-related	1	0	2	7	0	0.170
LMO1/2-TRA	0	0	0	4	0	0.110
other TCR-related	1	0	2	3	0	0.777
NUP-related	10 (41.7%)	3 (33.3%)	2 (5.9%)	3 (6.5%)	1 (5.9%)	<0.001
SET-NUP214	8 (33.3%)	1 (11.1%)	0	1	0	<0.001
NUP214-ABL1	0	0	2	2	1	0.750
NUP98-related	2 (8.3%)	2 (22.2%)	0	0	0	0.003
KMT2A-related [6]	1	0	1	1	1	0.916
PICALM-MLLT10	1	0	0	2	1	0.707
ZBTB16-ABL1	0	1	1	0	0	0.123
Other fusion genes	1	2	4	7	3	0.577
Gene over-expression						
HOX-related	20 (83.3%)	7 (77.8%)	8 (23.5%)	17 (37.0%)	9 (52.9%)	<0.001
TLX1	0	0	1	1	1	0.771
TLX3	1	1	2	10	4	0.112
HOXA	19 (79.2%)	6 (66.7%)	6 (17.6%)	10 (21.7%)	9 (52.9%)	0.000
LMO1	2	0	2	5	3	0.562
LMO2	5	0	4	4	1	0.370
LYL1	14 (58.3%)	3 (33.3%)	3 (8.8%)	6 (13.0%)	3 (17.6%)	<0.001
TAL1	4	0	10	13	3	0.287

SLC17A9-short	0	0	21 (61.8%)	28 (60.9%)	9 (52.9%)	<0.001
MEF2C	20 (83.3%)	4 (44.4%)	7 (20.6%)	2 (4.3%)	0	<0.001
Gene mutations						
NOTCH1 / *FBXW7* (C1)	19	8	23	40	12	0.237
Signaling Pathways (C2)	17	6	18	24	12	0.284
JAK-STAT pathway	8	3	8	9	5	0.712
RAS pathway	11 (45.8%)	2 (19.2%)	5 (14.7%)	6 (13.0%)	1 (5.9%)	0.006
PI3K pathway	0	0	4 (11.8%)	6 (13.0%)	6 (35.3%)	0.011
PTEN	1	1	5	3	3	0.481
Epigenetic Factors (C3)	20 (83.3%)	6 (66.7%)	19 (55.9%)	21 (45.7%)	12 (70.6%)	0.032
PHF6	8	2	6	10	5	0.676
Transcription Factors (C4)	10	2	9	14	3	0.514

[a] The relapse rate is calculated based on the number of the cases with complete remission.

[b] *KMT2A*-related fusions include *KMT2A-MLLT1* (1 case), *KMT2A-MLLT4* (1), *KMT2A-ELL* (1), and *KMT2A-CBL* (1), respectively.

Table S3. Specific gene signatures of Pro, Pre, Cortical, Medullary and ETP immunophenotypic subgroups based on gene expression signal

Pro		Pre	Cortical	Medullary	ETP			
CD8B	CDRT1	PARD3B	TSPYL2	TMEM213	BLNK	PPM1J	CDH13	PRICKLE2
CD4	PTPRM	CDH9	GADD45G	CLEC9A	PRX	ACOT11	SCARA5	HTRA3
POU3F2	SCN4B	ADAMTS8	BNIPL	PROZ	FAM160A1	CYP1B1	CD163	C1QTNF4
CD8A	SPR	TENM3	RGMB	ATP6V0A4	KLHL4	C1QA	EGFL7	CYTL1
ATP6AP1L	ITIH6	TMEM121	TP53INP2	ADAM23	TF	GPX8	CTGF	NOVA2
CD1A	EDARADD	LAMC3	NNAT	RSAD2	TIFAB	CCDC50	LAMA4	EPHA2
RAG1	CHRNA3	CAPN12	SPATA21	LIPG	PTK2	FAM46A	LPCAT2	IGLL1
LYST	CPNE8	TRPV5	GADD45A	OAS1	IRF8	PRODH	NLRP7	DUSP27
CD1D	KLK1	PLA2G4F	GPR3	RNF157	CP	LDLRAD3	ARHGEF17	HLA-DQB1
CEP128	TCEAL2	MOBP	COL6A2	RNF168	TNFRSF11A	FCER1A	FNDC1	CLEC4M
TRHDE	ASAH2	SYN3	B3GNT4	MX1	OLFML2B	BTK	EGFR	CX3CL1
MAP6D1	HOMER1	CPNE9	CACNG4	FFAR2	LDLRAD2	GUCY2D	IL33	SLC22A3
AMER2	ULBP1	OSBPL10	TRAF4	G0S2	MCTP2	P2RY2	SCHIP1	KLHL13
GJB6	DPYSL5	HTRA4	MATN1	ACE	SMOC1	LTK	BCAN	ANO2
FGFR3	GPC3	CYP26C1	FSCN3	CTSH	ZDHHC14	NOG	KIT	CADPS2
SIRPG	WNK2	THPO	TMEM88	HSPA6	VCAM1	GLYATL2	MLC1	CACNA2D3
ADAMTS17	ARHGAP19-SLIT1	COMP	GATA6	RGMA	APOE	FMO2	FLT3	ADRA2A
PITPNM2	PDE10A	CATSPERD	PPP1R15A	PGLYRP2	SLCO2B1	LYN	GNG7	APOB
KCNK9	SNAP25	SLC45A1	CYP4X1	LAMA2	CLEC4C	MYLK	PLA1A	TBX2
SLC29A1	ANKRD1	COL5A2	CYP4F11	PTGIS	CXCL11	FOXC1	GNG12	ASCL4
HIST2H3A	CNNM1	MYBPC3	MAFB	CLEC4D	SUCNR1	TNFSF13B	MN1	PTGFR
MNS1	SUSD4	GLP2R	IBA57-AS1	LIF	ANKRD65	FZD4	NAV3	CSRP3
DMPK	PPP1R3C	PPFIBP2	DPPA4	ROR1	NRP1	BMP2	CD33	GP9
FSTL4	FBXO27	BEGAIN	AXDND1	SYT11	ADRB2	BAALC	SH3BP4	TBL1Y
DAAM2	AKAP12	INSRR	POU5F1B	ROBO2	CSF1	COL8A1	TNR	NYNRIN
GJB2	NINL	MSR1	IER3	CLEC4E	NEK6	ICAM5	LPL	ACSM5
GCSAM	ELOVL4	FGF18	LRRC10B	PLIN2	C1QC	IL13RA1	KIAA0087	OPHN1
MEST	ASAH2B	NFASC	TTC39A	RPRML	AK4	CD209	SGCD	HTR1F
CD1C	B3GAT1	SPAG17	TLE2	CHAT	ITGA9	ABCA3	LUM	EFS
ACOXL	LGALS2	CELSR1	PDGFRB	RGS17	LBP	MOB3B	CSRP2	LGR5
PLAG1	OLFM1	GNAT2	IRGC	FGF14	CCDC80	PROSER2	NR2F1	WNT6
FYB	DTX1	CYP27B1	KLHL35	SLC7A11	SAMD11	PLTP	CCL1	EDIL3
DIO2	TREH	PCDHGA3	FOXA1	B3GALT1	KANK2	NOXA1	PARVA	COL21A1
SLAMF1	DRAXIN	SIGLEC11	CACNA1I	ISG15	PXDC1	IRGM	SERPINB6	SLC6A1
AQP6	STEAP1B	ALPK3	PDE4C	SEMA4A	CHL1	CHRD	DHRS9	CYP27C1
SMPD3	GAD2		SERTAD1	F7	FCRLA	PLXNB2	CAPNS2	DUSP15
AQP3	ANTXR1		VWA5A	HPGD	SVEP1	SPIC	TM4SF18	PRSS57
GSC	OR10K1		PLEKHG3	CLSTN2	LRRK1	BMP5	MEF2C	PPBP
SH3GL3	PTPN3		JAKMIP3	ARHGAP6	HLA-DMA	MS4A6A	NCKAP5	CEBPA
RAG2	UNC45B		COL9A3	LDOC1	HLA-DPB1	RAB3C	VTCN1	PSD3
PCSK5	SLIT1		MTUS2	STXBP5L	TEK	TENM4	CFI	FAM69C
NLRP14	CHRNB3		PDE2A	L1CAM	SHD	FMO3	RSPO1	PRKG1
KIRREL	GUCY1A2		OTUB2	ANXA3	PTGER2	ADAMTS5	WNT5A	HLA-DRB5
NPAS2	RAET1L		ADAMTS7		CXCL12	EPHB3	DLX1	ELN
PRG4	IGSF1		BAG3		DEXI	NRGN	GPT2	FABP4
FAM163B	TMPRSS2		TUBB2A		FUT7	MXRA5	SEZ6L	GABRE
TPPP3	PRKCZ		USP2		VSIG2	CLEC4G	ADAMTS9	ACSS3
PTCRA	OR10T2				NGFR	FAM43A	IL10	ITGBL1
FAM182B	HMGCS2				C1QB	HSH2D	STAP1	CAMK2N2

Pro		Pre	Cortical	Medullary	ETP			
SHISA9	PAX9				CD5L	SLC45A3	CCL13	IBSP
METRN	MYO3A				TNC	ADCY9	LINGO2	CNTN1
CX3CR1	TEAD4				SPARC	ARHGEF15	LAMB4	SHOX2
KCNJ4	SERTAD4				MAPK12	CDH5	S100A16	SEC14L5
CCDC78	NCKAP1				IRF5	GFRA2	HRH4	LAMP5
GRB7	MAT1A				APP	TBXA2R	TM4SF1	EGFL6
FASLG	ARMC4				HLA-DMB	MEIS3	PDE4B	PROM1
FAM3B	GPR63				ACOX2	LIFR	ARHGAP22	DCLK1
FGR	GLB1L2				ARHGEF40	PLXNA4	DLX2	TBX3
DCLK3	CLEC10A				LYVE1	COL6A1	LAPTM4B	SOX9
CD1E	ESRP1				DNASE1L3	SPATA12	NPAS3	MRO
BTN1A1	DDAH1				MET	STAB1	CPA3	EYA1
HIST3H2BB	CCDC8				ITIH5	CD300LF	SALL4	EGFLAM
CPA5	HPCAL4				C7	TCTEX1D1	EMCN	SLC6A11
SCRN1	SYT1				FAM180B	HTR7	OPRK1	ZNF536
POF1B	TRPC3				FKBP10	SRPX	NTRK2	PIRT
HS6ST2	MAL				LHFPL2	MPO	TIE1	PTH2
GRM8	ACSM4				P2RY6	STYK1	HOXC4	MS4A4E
MST1R	SPTSSB				ABCC9	FRK	RAMP3	LHX6
HIST1H1B	ADAM33				AXL	FGFR2	WFDC1	SFRP1
NTNG1	MPPED2				CD74	HLX	ID4	TENM2
KLRG2	CAMKV				DOCK6	DLC1	BCAR1	WNT9A
ROR2	A1CF				KYNU	MYCL	SMOC2	CXCL10
AXIN2	LINC00346				AHNAK2	CLNK	PDZRN4	TRH
RBMXL2	HES4				RNASE1	MGLL	FER1L6	CACNA2D1
CHN1	OR10R2				ESM1	MMRN1	VWA1	CHRNA7
XKR7	MOCS1				CSPG4	HLA-DRB1	CYGB	EGF
THEMIS	HEY2				LILRA4	ZC3H12C	ALOX15B	LDHAL6B
LIM2	CHST3				DNAJC5B	PPP2R2B	KIF17	AMBN
CPS1	RBM24				PLD4	SDK2	SORCS1	FCN2
GPR157	KCNS3				GAPT	PTGS1	MACC1	CCL8
RIPK4	LPIN3				B3GNT7	UNC79	MROH7	MMP7
PTMS	SLC6A15				NPR3	SMIM3	FAT3	PDGFC
KCNC2	TBX20				LPO	ITGAD	GGT5	TWIST1
SEPT8	AVPR1A				CCR2	TMEM37	HOXC11	SLC7A10
CD1B	ANKFN1				EMX2	COL4A2	TDO2	RHOJ
OR2D3	NRXN3				VWF	CLEC2A	NPTX1	TMEM196
SYDE2	TMEM155				FOLR2	TJP1	SLC22A10	PCDH17
FTCDNL1	PTPN13				APBA1	CUX2	RNF180	GJA1
SIX5	LRRIQ1				IGFBP3	TNS3	MPV17L	INSL5
JAKMIP1	ADAMTSL1				LILRB4	KCNK10	UTS2B	EQTN
DAB2IP	FAM183A				SLC8A3	CDH11	DCN	DRGX
SCN1A	MUC13				ALDH1A3	ATP8B4	KDR	FOXF1
NOTCH3	NLGN4X				LIMCH1	PRLR	OLIG2	MMP16
ADAMTSL3	BMPR1B				KIF26B	KCNJ8	PPIC	CYP2C8
CPA4	MAP2				CFD	APOD	CPN2	COL2A1
PAK3	SLC1A1				HLA-DPA1	COL14A1	PDGFRA	CDH10
KIAA2022	ABCG4				IGFBP7	GABRA2	ITGA8	PF4V1
KCNG3	TFAP2C				TNNI2	MEGF10	MB	
TTC16					LILRB5	EBI3	TMEM47	
APBB2					CMKLR1	TTLL10	CHRFAM7A	

Table S4. Clinical and genetic differences between adult and pediatric T-ALL patients

Characteristics	adult (n=61)	childhood (n=69)	*P* value
WBC count			0.004
>=100×10^9/L	15 (24.6%)	34 (49.3%)	
<100×10^9/L	46 (75.4%)	35 (50.7%)	
ETP	17 (27.9%)	7 (10.1%)	0.009
Complete Remission	46 (75.4%)	64 (92.8%)	0.006
Fusion genes			
SET-NUP214	8 (13.1%)	2 (2.9%)	0.029
Over-expression			
LYL1	19 (31.1%)	10 (14.5%)	0.023
TAL1	8 (13.1%)	22 (31.9%)	0.011
SLC17A9-short	17 (27.9%)	41 (59.4%)	<0.001
HOXA	33 (54.1%)	17 (24.6%)	0.001
MEF2C	26 (42.6%)	7 (10.1%)	<0.001
Mutations			
Signaling Pathways (C2)	47 (77.05%)	30 (43.5%)	<0.001
Epigenetic Factors (C3)	47 (77.0%)	31 (44.9%)	<0.001

Reference:

1. Larson RA, Fretzin MH, Dodge RK, & Schiffer CA (1998) Hypersensitivity reactions to L-asparaginase do not impact on the remission duration of adults with acute lymphoblastic leukemia. *Leukemia* 12(5):660-665.
2. Thomas DA*, et al.* (2010) Chemoimmunotherapy with a modified hyper-CVAD and rituximab regimen improves outcome in de novo Philadelphia chromosome-negative precursor B-lineage acute lymphoblastic leukemia. *Journal of clinical oncology : official journal of the American Society of Clinical Oncology* 28(24):3880-3889.
3. Gu LJ*, et al.* (2008) Clinical outcome of children with newly diagnosed acute lymphoblastic leukemia treated in a single center in Shanghai, China. *Leukemia & lymphoma* 49(3):488-494.
4. Liu Y*, et al.* (2009) Cost of childhood acute lymphoblastic leukemia care in Shanghai, China. *Pediatric blood & cancer* 53(4):557-562.
5. Liu YF*, et al.* (2016) Genomic Profiling of Adult and Pediatric B-cell Acute Lymphoblastic Leukemia. *EBioMedicine* 8:173-183.
6. Kim D, Langmead B, & Salzberg SL (2015) HISAT: a fast spliced aligner with low memory requirements. *Nature methods* 12(4):357-360.

7. Anders S, Pyl PT, & Huber W (2015) HTSeq--a Python framework to work with high-throughput sequencing data. *Bioinformatics* 31(2):166-169.

8. Nicorici D*, et al.* (2014) FusionCatcher - a tool for finding somatic fusion genes in paired-end RNA-sequencing data. *bioRxiv*.

9. McPherson A*, et al.* (2011) deFuse: an algorithm for gene fusion discovery in tumor RNA-Seq data. *PLoS computational biology* 7(5):e1001138.

10. Lilljebjorn H*, et al.* (2016) Identification of ETV6-RUNX1-like and DUX4-rearranged subtypes in paediatric B-cell precursor acute lymphoblastic leukaemia. *Nature communications* 7:11790.

11. Atak ZK*, et al.* (2013) Comprehensive analysis of transcriptome variation uncovers known and novel driver events in T-cell acute lymphoblastic leukemia. *PLoS genetics* 9(12):e1003997.

12. McKenna A*, et al.* (2010) The Genome Analysis Toolkit: a MapReduce framework for analyzing next-generation DNA sequencing data. *Genome research* 20(9):1297-1303.

13. Dobin A*, et al.* (2013) STAR: ultrafast universal RNA-seq aligner. *Bioinformatics* 29(1):15-21.

14. Koboldt DC*, et al.* (2009) VarScan: variant detection in massively parallel sequencing of individual and pooled samples. *Bioinformatics* 25(17):2283-2285.

15. Wilm A*, et al.* (2012) LoFreq: a sequence-quality aware, ultra-sensitive variant caller for uncovering cell-population heterogeneity from high-throughput sequencing datasets. *Nucleic acids research* 40(22):11189-11201.

16. Jiang L*, et al.* (2015) Exome sequencing identifies somatic mutations of DDX3X in natural killer/T-cell lymphoma. *Nature genetics* 47(9):1061-1066.

17. Kiran A & Baranov PV (2010) DARNED: a DAtabase of RNa EDiting in humans. *Bioinformatics* 26(14):1772-1776.

18. Ramaswami G & Li JB (2014) RADAR: a rigorously annotated database of A-to-I RNA editing. *Nucleic acids research* 42(Database issue):D109-113.

19. Neumann M*, et al.* (2015) Mutational spectrum of adult T-ALL. *Oncotarget* 6(5):2754-2766.

20. Van der Meulen J, Van Roy N, Van Vlierberghe P, & Speleman F (2014) The epigenetic landscape of T-cell acute lymphoblastic leukemia. *The international journal of biochemistry & cell biology* 53:547-557.

21. Girardi T, Vicente C, Cools J, & De Keersmaecker K (2017) The genetics and molecular biology of T-ALL. *Blood* 129(9):1113-1123.

22. Mullighan CG (2014) The genomic landscape of acute lymphoblastic leukemia in children and young adults. *Hematology. American Society of Hematology. Education Program* 2014(1):174-180.

23. Love MI, Huber W, & Anders S (2014) Moderated estimation of fold change and dispersion for RNA-seq data with DESeq2. *Genome biology* 15(12):550.

24. Anders S, Reyes A, & Huber W (2012) Detecting differential usage of exons from RNA-seq data. *Genome research* 22(10):2008-2017.

25. Soneson C, Matthes KL, Nowicka M, Law CW, & Robinson MD (2016) Isoform prefiltering improves performance of count-based methods for analysis of differential transcript usage. *Genome biology* 17:12.

26. Schwab CJ*, et al.* (2013) Genes commonly deleted in childhood B-cell precursor acute lymphoblastic leukemia: association with cytogenetics and clinical features. *Haematologica* 98(7):1081-1088.

27. Thieme S & Groth P (2013) Genome Fusion Detection: a novel method to detect fusion genes from SNP-array data. *Bioinformatics* 29(6):671-677.

28. Bene MC*, et al.* (1995) Proposals for the immunological classification of acute leukemias. European Group for the Immunological Characterization of Leukemias (EGIL). *Leukemia* 9(10):1783-1786.

29. Alvarnas JC, *et al.* (2015) Acute Lymphoblastic Leukemia, Version 2.2015. *Journal of the National Comprehensive Cancer Network : JNCCN* 13(10):1240-1279.